Combined heat and mass transfer for drying ceramic (shell) body

Zawati Harun[1], D.T. Gethin[2] and R.W. Lewis[2]
[1]University Tun Hussein Onn, Parit Raja, 86400,
Batu Pahat, Johor, Malaysia
(Phone: +660-7453 7717; Fax: +660-7453 6080)
E-mail: zawati@uthm.edu.my, zawati73@yahoo.com
[2]Civil and Computational Engineering Centre, University of Wales,
Singleton Park, Swansea, SA2 8PP, UK
E-mail: D.T.Gethin@swansea.ac.uk
E-mail: R.W.Lewis@swansea.ac.uk

ABSTRACT
In the present work, a two-dimensional numerical model of heat and mass transfer for the convective drying of ceramic porous system was developed. The governing system of fully coupled non-linear partial differential equations describing the process was derived from a mechanistic approach. A formulation including hygrothermal and moisture transport in soil was adopted as the basis for further development in this work. The calculation results for drying of a ceramic brick showed that the model presented is in good agreement with other studies that have been reported previously in the drying of porous material. Further investigation on the shell drying agrees well with the most drying mechanism of ceramic porous body. The influence of material parameter on the drying profile is taken into consideration by carrying out some investigation on the material sensitivity study.

Keywords: A two-dimensional numerical model; Drying of ceramic porous; Drying mechanism

1. INTRODUCTION

Within investment casting, the drying process is one of the most important stages in ceramic shell build up during which a number of ceramic layers are added to form the shell. Layer drying has a direct impact on the process time and a number of layers are added in order to get sufficient strength. The ceramic shell attains its pre-final strength during the drying process, followed by firing during which the diffusion process forms a bond to achieve a hard and very strong body. An improper drying process will cause cracks and thermal expansion due to the excess moisture that was not removed during the drying process. Therefore drying rate and duration plays an important role in ceramic shell build up and was considered in this work. Drying of moist porous solids is a complicated process involving simultaneous, coupling of heat and mass transfer phenomena in a medium that exhibits a fine porous structure. The mechanism of heat and mass transfer in porous media is always related to moisture content, temperature variation and others physical properties in a nonlinear way. This makes the important material variables that characterise this process difficult to

measure. However with the help of a reliably realistic mathematical model of the drying process, the task becomes more manageable. Essentially, there are two approaches that are used to model the process, often attributed to Whitaker [1] and Luikov [2]. Whitaker's concept enables the expression of the moisture and heat transport of each phase (solid, liquid and vapour plus inert gas) in terms of average field quantities at the microscopic level. The assumption on the physical properties of the porous medium can be associated with mathematical field variables which in most cases can be derived from empirical and analytical approaches. This constitutive relationship can be considered as being a 'material model' as in many instances this can be directly measured within laboratory experiments. The Luikov model is based on irreversible thermodynamics and its theory provides a well-established model in the treatment of simultaneous heat and mass transfer for drying based on the extensive work that has been done previously [3,4]. Although such a treatment makes the process easily understood, it is more difficult to obtain the coefficient parameters that Luikov introduced in the governing equations of heat and mass transfer [4].

By using the volume average method, Whitaker [1] applied transport theory to porous media within a continuum framework. Their coefficients are easy to obtain and understand since vapour diffusion, capillary action, evaporation-condensation effects, Darcy flow and other actions are not considered individually. These are linked together leading to a thermodynamic and also porous transport formulation that is coupled. Thus, these equations are now well established and have been applied in drying process simulations that include both hygroscopic [5-8] and nonhygroscopic material [9-11]. The objective of this work is to develop the coupled heat and moisture governing equation (along with the gas transport consideration) for a ceramic shell body, based on the hygrothermal and thermodynamic transport properties. The presence of coupled heat, mass and gas transport in a two-dimensional framework is an extension of the approach presented in [8,9]. Others considerations, such as the expression of heat and mass transfer coefficients influenced by the evaporation front is also included.

2. THEORETICAL FORMULATION

The theoretical formulation of the heat and mass balance equations used here is based on the work by Ben Nasrallah [9], Whitaker [3] and others [1,4,5]. Based on the above analysis, the governing equations of the model are expressed in terms of the chosen state variables; pore water pressure, P_l temperature, T and gas pressure, P_g.

The drying conservation law of mass flow in the open porous network can be obtained by taking consideration of each interaction of its component phases, namely liquid and vapour interaction. The time derivative of moisture (liquid and vapour) transport as given below in eqns (1-2) reflects the gradient of liquid flux, the influence of vapour pressure gradient due to the vapour bulk flow and gas pressure gradient.

$$\text{For the liquid: } \frac{\partial \phi \rho_l}{\partial \mathrm{t}} = -\frac{\partial \rho_l v_l}{\partial x} - \dot{m} \tag{1}$$

$$\text{For the vapour: } \frac{\partial \phi \rho_v S_g}{\partial \mathrm{t}} = -\frac{\partial \rho_v v_g}{\partial x} - \frac{\partial \rho_v v_v}{\partial x} + \dot{m} \tag{2}$$

In eqn (1), liquid occupies the portion of pores (ϕ) within the structure and the rate of transport of liquid through the pores combined with the evaporation rate ($\dot{m}$) balances the

liquid depletion rate. A similar principle applies to the vapour phase (in eqn (2)). The vapour phase is transported by the vapour velocity itself, plus the component of vapour that is transported by the air flow and condensation rate ($\dot{m}$). The depletion rate accounts for the saturation level of liquid (S_l) and gas (S_g) within the porous structure. The liquid and vapour transport, summed together form the mass balance equation for the moisture phase.

$$\frac{\partial(\phi\rho_l S_l)}{\partial t} + \frac{\partial(\phi\rho_v S_g)}{\partial t} = -\nabla(\rho_l \mathrm{v}_l) - \nabla(\rho_v \mathrm{v}_v) - \nabla(\rho_v \mathrm{v}_g) \tag{3}$$

In eqn (3), water and gas velocity can be easily derived from Darcy's law

$$\mathrm{v}_1 = \frac{-\mathrm{K}k_l}{\mu_l}\nabla P_l + \nabla Z \tag{4}$$

$$\mathrm{v}_g = \frac{-\mathrm{K}k_g}{\mu_g}\nabla P_g \tag{5}$$

where Z is the vertical elevation from a datum, K is the intrinsic permeability, k_l and k_g are liquid and gas permeability.

Transport in the vapour state by diffusion is given by;

$$\mathrm{v}_v = \frac{-\phi S_g D_{atm} v\alpha}{\rho_v}\cdot\nabla\rho \tag{6}$$

This equation reflects the physical principle of vapour diffusion due to the vapour pressure difference in the moist porous media with respect to the proportion of gaseous mixture. In eqn (6), v, α are the mass flow factor and tortuosity factor as given in [10]. $\mathrm{D}_{\mathrm{atm}}$ is the molecular diffusivity of water vapour through dry air, and is given in reference [8].

To facilitate the calculation of temperature, the energy equation for the whole medium is given as;

$$\frac{\partial\left(\left(1-\phi\right)C_p\rho_s + \phi S_g\rho_v L\right)}{\partial t} = \nabla(\lambda\nabla T) - \nabla(\rho_v \mathrm{v}_v + \rho_v \mathrm{v}_g)L - \nabla \left(\sum_{i=a,l,v}(T-T_r)\rho_i C_{pi}\mathrm{v}_i\right) \tag{7}$$

The first term on the right side in eqn (7) indicates the energy transfer through conduction in liquid, gas and solid of porous network. The second term involves the vapour movement due to the latent heat contribution. The last term shows the heat transfer between a surface and a moving fluid at different temperatures via phase convection.

The contribution due to gas flow may be found by applying a mass balance to the gas portion within the pores of ceramic body. This reflects the physics that the time derivative of the gas content is equal to the spatial derivative of the gas flux plus the condensation term and is expressed as

$$\frac{\partial \phi S_g \rho_g}{\partial t} = -\nabla\left(\rho_g v_g\right) + \dot{m} \tag{8}$$

By substituting the evaporation term in eqn (2) into eqn (8) reduces the equation to;

$$\frac{\partial\left\{\phi S_g \rho_a\right\}}{\partial t} = \nabla\left(\rho_a v_g\right) - \nabla\left(\rho_v v_v\right) \tag{9}$$

The right hand side of eqn (9) includes a mechanism from two effects which are the dry air transport driven by gas pressure gradient and the vapour pressure gradient that arises from vapour diffusion into the air. The pressure and density of the gas accounts for the dry air and vapour mixture that is dependent on the humidity within the ceramic matrix as well as the humidity convection at the surface of the body. In this problem, the gas phase is modelled as an ideal gas that is composed of dry air and vapour.

3. THERMODYNAMIC RELATIONSHIP

The existence of a local equilibrium at any point within the porous system is assumed. The equilibrium vapour pressure can be approximated by Kelvin's equation. This equation shows that the equilibrium of water vapour, P_v differs from the saturation pressure, P_{vs}, due to the curvature of the interface between capillary or hygroscopic water and the gas phase inside the pores of the medium. Given that the relative humidity within the porous matrix is given by

$$(rh) = \exp\left(-\frac{P_c}{\rho_l R_v T}\right) = \exp\left(-\frac{P_g - P_l}{\rho_l R_v T}\right) \tag{10}$$

The partial vapour pressure can be calculated as a function of local temperature and relative humidity using the relationship

$$P_v = rh\left(P_{v(sat)}\right) \tag{11}$$

where the saturation vapour pressure, $\left(P_{v(sat)}\right)$ may be estimated using the saturated vapour density as a function of temperature and is given in [12]. This has been fitted to the vapour-pressure–temperature data from the steam tables. The degree of saturation S_l (considering together hygroscopic region water and capillary water, if the latter is contained in the pores) is an experimentally determined function of capillary pressure and temperature [13]. In many hygrothermal and soil transport problems, this is expressed as [14];

$$S_l = \frac{\left(S_l\right) - \left(S_l\right)_{irr}}{\left(S_l\right)_{sat} - \left(S_l\right)_{irr}} = \left(\frac{1}{1 + \left(\alpha\varphi(T)\right)^n}\right)^m \tag{12}$$

where the parameters α, n and m are three different porous material properties that are directly dependent on the shape of the water retention curve. Determination of these material parameters is a key step based on the several documented works [15,16]. These show

hysteresis of the saturation curve in drying and wetting of clay soil and brick materials. The appropriateness of this will be addressed later within this research programme. The relative permeability expression for water and gas using Mualem's model that has been developed for soils and implemented in hygrothermal research [15,16], was also implemented in this model (eqns (13-14)). In the latter work, these relative permeability properties were measured under an isothermal condition which is the most appropriate for drying of a ceramic shell body.

$$k_l\left(S_l\right) = \sqrt{S_l}\left(1-\left(1-S_l^{1/m}\right)^m\right)^2 \tag{13}$$

$$k_g\left(S_l\right) = \sqrt{1-S_l}\left(1-S_l^{1/m}\right)^{2m} \tag{14}$$

4. MATERIAL DATA FOR THE CERAMIC (SHELL) BODY

In this work the ceramic shell body was considered to have the same properties as a nonhygroscopic brick and cement paste [8, 9, 16]. This is because the drying of the ceramic shell is far below the temperature at which bound water becomes a consideration [17].

5. BOUNDARY CONDITION

The general boundary condition for convective mass and heat transfer are given by:

$$\mathrm{J_m} = h_m\left(P_\infty^v - P_f^{\,v}\right) \tag{15}$$

$$\mathrm{J_h} = h_T\left(T_\infty - T_f\right) \tag{16}$$

This captures the physical process where the water vapour pressure which is related to the humidity is the driving force that transfers moisture out from the body to the surrounding air. The analogy between heat and mass transfer at the surface of a drying material is covered in standard textbooks [18] where the mass transfer coefficient is applicable principally in the falling rate period. In this work the analogue relationship given by Nissan *et al.* [19] was used. This captures the dependence of heat and mass transfer coefficients including the influence of surface water content. The specific boundary conditions that apply will be presented fully in connection with the case studies in section 7.

6. SOLUTION OF GOVERNING EQUATIONS AND NUMERICAL METHOD

The coupled heat and mass transfer equations presented above apply to spatial domains from one to three dimensions. Generally, in two dimensions this can be written in a matrix form as follows;

$$\left[C\left(\Phi\right)\right]\frac{\partial}{\partial t}\left\{\Phi\right\} = \nabla\left(\left[K_{cx}\left(\nabla\Phi\right)\right]i_x + \left[K_{cy}\left(\nabla\Phi\right)\right]i_y\right)\left\{\Phi\right\} + R\left(\nabla Z\right) \tag{17}$$

where $\{\Phi\} = \{P_l, T, P_g\}$ is the column of unknowns; $[C]$, $[K_{cx}]$ and $[K_{cy}]$ are 3×3 matrices. Each element of the matrix, is a coefficient for the unknown $\{\Phi\}$; i_x and i_y are the unit direction vectors. This second order non-linear coupled partial differential equation set is then discretised using the finite element method. By minimising the residual error using the Galerkin method, followed by the application of Greens theorem to the dispersive term involving second order derivatives, this combined equation set can be expressed in the following form.

$$\underline{K}(\Phi)\underline{\Phi} + \underline{C}(\Phi)\dot{\underline{\Phi}} + \underline{J}(\Phi) = \{0\} \tag{18}$$

where,

$$K = \begin{bmatrix} \underline{K}_{11} & \underline{K}_{12} & \underline{K}_{13} \\ \underline{K}_{21} & \underline{K}_{22} & \underline{K}_{23} \\ \underline{K}_{31} & \underline{K}_{32} & \underline{K}_{33} \end{bmatrix} \quad \underline{C} = \begin{bmatrix} \underline{C}_{11} & \underline{C}_{12} & \underline{C}_{13} \\ \underline{C}_{21} & \underline{C}_{22} & \underline{C}_{23} \\ \underline{C}_{31} & \underline{C}_{32} & \underline{C}_{33} \end{bmatrix}$$

$$\dot{\underline{\Phi}} = \begin{Bmatrix} \dfrac{\partial \underline{P}_{ls}}{\partial t} \\ \dfrac{\partial \underline{T}_s}{\partial t} \\ \dfrac{\partial \underline{P}_{gs}}{\partial t} \end{Bmatrix} \quad \underline{\Phi} = \begin{Bmatrix} \underline{P}_{ls} \\ \underline{T}_s \\ \underline{P}_{gs} \end{Bmatrix} \quad \underline{J} = \begin{Bmatrix} \underline{J}_1 \\ \underline{J}_2 \\ \underline{J}_3 \end{Bmatrix}$$

In which typical elements of the matrix are;

$$\underline{C}_{ij} = \sum_{s=1}^{n} \int_{\Omega^e} C_{ij} N_r N_s d\Omega^e \qquad \underline{K}_{ij} = \sum_{s=1}^{n} \int_{\Omega^e} K_{ij} \nabla N_r \nabla N_s d\Omega^e$$

$$\underline{J}_i = \int_{\Omega^e} K_{i4} \nabla N_r \nabla z d\Omega^e - \int_{\Gamma^e} N_r \underline{J}_i \bar{n} d\Gamma^e$$

where (i, j = 1,2,3) and $\bar{n}$ is the outward normal vector to the element boundary, Γ^e of the element body, Ω^e. The transient matrix and nonlinear second order differential equations above were then solved by using a fully implicit backward time stepping scheme along with a Picard iterative method to account for the non-linearity [20] in the phenomenological coefficients, $\underline{K}$, $\underline{C}$ and $\underline{J}$. The system of simultaneous equations within each iteration resulting from the above method was then solved using a Skyline solver [21].

7. RESULT AND DISCUSSION

7.1. ONE DIMENSIONAL CASE STUDY AND VALIDATION

Testing of the model for verification was performed for a nonhygroscopic material within a one-dimensional framework. The geometry was described by a brick comprising 227mm long × 104mm wide × 32mm thick. The heat transfer and drying process takes place at the top exposed surface that comprises a section 227mm long by 104mm wide. The remaining

Table 1 Physical and transport properties of the ceramic body

ρ_s	ϕ	K	Cp	Λ	L	S_{irr}
2000	0.12	1×10^{-14}	925	1.8	2.4×10^6	0.09

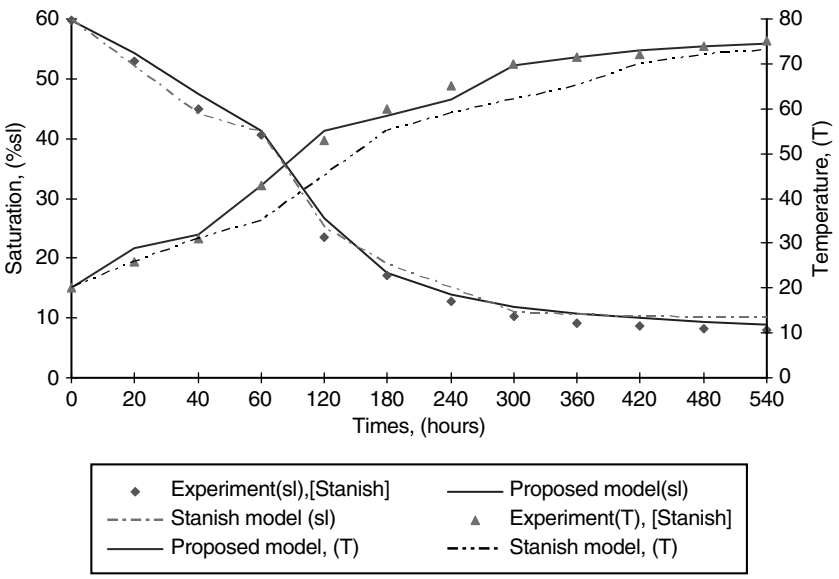

Figure 1 Liquid saturation and temperature changing over the drying time.

surfaces are perfectly insulated and are impermeable. This enables validation against the work by Stanish *et al*. [8] in which he reported both experimental data as well as results from simulation. The relevant material properties are presented in the Table 1 and the matrix is assumed to be fully saturated at the commencement of the drying process. The initial temperature is uniform at 20°C and the gas pressure is uniformly at the ambient condition throughout the matrix. At the exposed surface, heat and mass transfer coefficients $h_T = 6$ W/m^2/K and $h_m = 0.008$ ms^{-1} at which the ambient temperature is 75°C and the relative humidity is set to 50% . The gas pressure is assigned to the ambient value.

Experimental data from [8] and simulation results are shown in Figure 1 in which moisture and temperature at the middle height of the brick are depicted over time. The experimental result shows that the moisture drops quickly at the beginning, corresponding to the constant drying rate period. During this stage the movement of liquid is maintained by the capillarity of the porous matrix. At the same time the temperature increases gradually starting from the top surface. At this point, the internal moisture transfer to the surface and the evaporation at the surface are in equilibrium, and the free water on the surface will be evaporated steadily and continuously. Over the drying duration, the saturation level decreases and at nearly 60 minutes, it displays the characteristics of a falling rate period where there is a reduction in the rate of moisture loss. Theoretically, the saturation level will recede continuously into the interior of the materials and the dry zone will extend

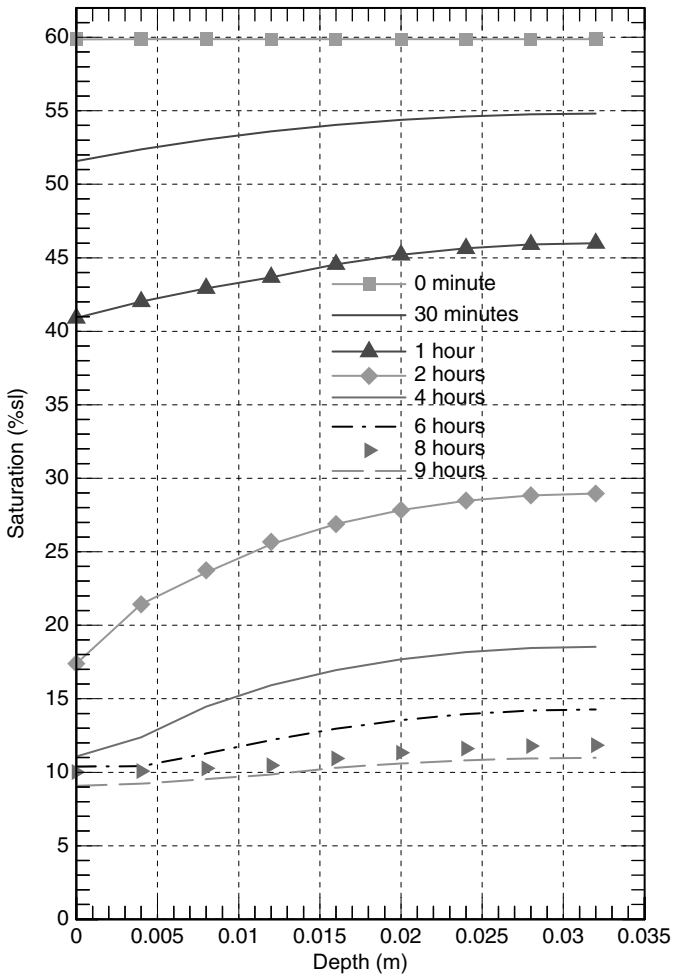

Figure 2 Saturation variation along the depth.

gradually. Normally this corresponds to a critical saturation of about 0.3 for most porous material [22]. This shows the start of the falling rate period. During this period the drying process will slow down and drying is now controlled by the water vapour movement. A comparison with experimental data is also displayed in Figure 1 where both simulations show very good agreement. In fact superior agreement has been achieved for the thermal characteristics, as the model proposed in this work take into account the latent heat contribution which is not presented in the numerical work by Stanish *et al.* [8]. This confirms the basis and quality of the simulation model that has been developed in this work and applied in this case study.

It is also useful to use the simulation to explore more fully the transient behaviour that takes place on a section through the brick. Figure 2, depicts the change in saturation over the brick depth at discrete times, where zero depth corresponds to the exposed top surface. This shows clearly the moisture gradient in the constant and falling rate periods and how it achieves a near uniform value of 90% after an extended period. An analogous pattern for

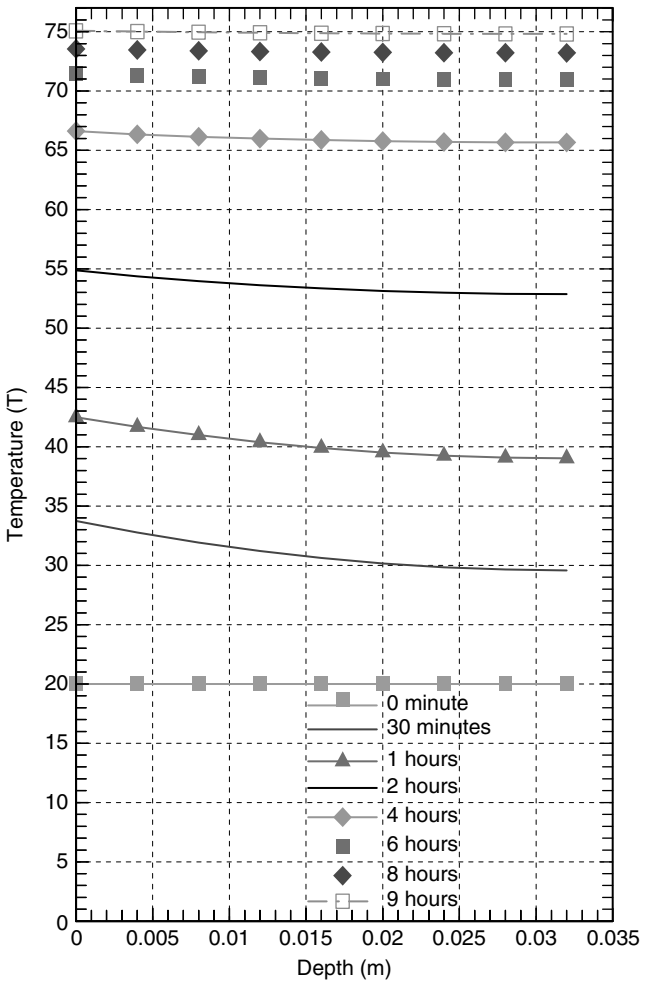

Figure 3 Temperature variation along the depth.

temperature is also exhibited in Figure 3, showing a temperature rise as a consequence of heat transfer from the ambient condition. Temperature increase is moderate during the constant rate period (up to 1 hour) and there is a big increment after falling rate period and finally small temperature change as the matrix achieves low levels of saturation, stabilizing towards the ambient condition of 75°C after extended drying.

The material model also incorporates the dependence of permeability on moisture content and this is displayed in Figure 4, where the permeability change starts to show a small reduction when nearing hygroscopic saturation. Also, as can be seen from Figure 4, the permeability properties drop close to zero at the saturation value of 0.1. This is due to failure of liquid transport by capillary action and this is no longer possible below the irreducible saturation level [23,24]. It has been found that the experimental detection of very low permeability is extremely difficult and it is generally taken as equal to zero in the drying process. Figure 5, also includes the variation of relative humidity within the porous matrix as a function of saturation. Above the critical saturation, the relative humidity remains close to a saturated

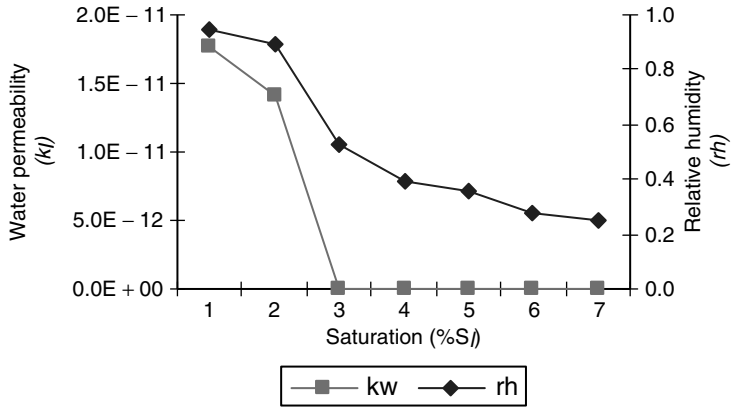

Figure 4 Permeability and relative humidity against saturation.

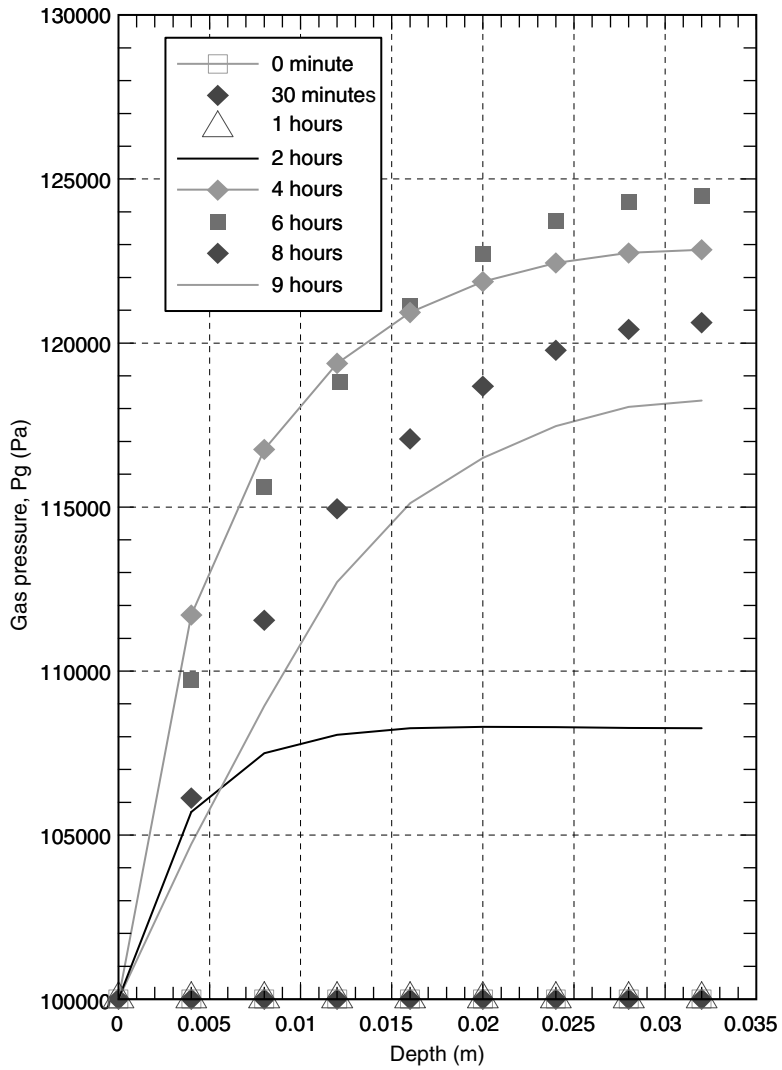

Figure 5 Gas pressure variation along the depth.

condition and below this value it reflects the falling rate condition where the vapour transport mechanism plays an important role in changing the local humidity. When near to irreducible saturation, the relative humidity just shows a very small change, indicating the minimum water content to which a material can theoretically be dried under the non hygroscopic condition.

The simulation also allows exploration of gas and pore water pressure changes that take place within the porous matrix. During the initial period, the pressure remains at a nearly constant level at atmospheric pressure. As drying proceeds and approaches the falling rate period where the temperature starts to increase there is a consequent rise in gas pressure. The pressure inside the sample increases to a maximum value at about 6 hours corresponding to the time when the temperature rise starts to slow down. Towards the end of the drying period, the gas pressure decreases, tending back to the ambient condition. A similar evolution in gas pressure during convective drying has been presented in several other works, such as in brick drying [9], in consolidating a slab of porous material [25], in drying of a concrete wall [26] and in drying of light concrete [27].

Pore water pressure evolution is shown in Figure 6. At the beginning, it remains at a nearly constant condition, but at a relatively high negative value. The near constant value

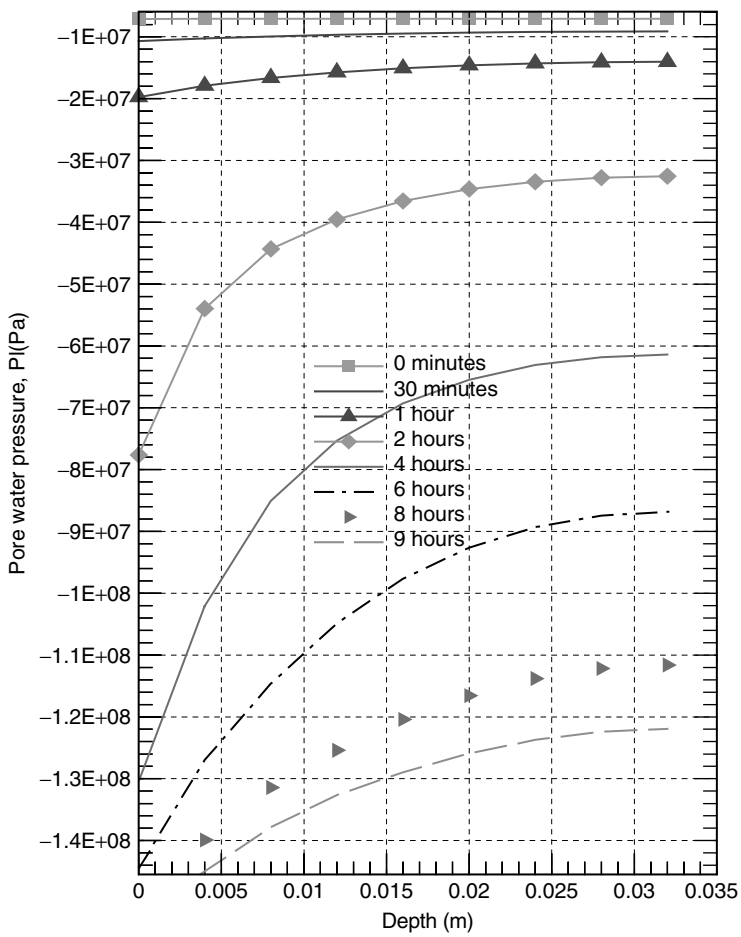

Figure 6 Pore water variation along the depth.

over the initial drying period indicates a regime of free water movement at nearly atmospheric ambient pressure. Over the falling rate period a big pressure decrement is recorded as drying proceeds within this range. This shows the condition when water recedes into the inner body and the capillary action is slowly diminished as water is strongly bonded to the porous matrix, consequently the pore water pressure becomes more negative at the free surface to facilitate moisture transport. Furthermore, reduction of capillary action in the porous body is accompanied by a gas pressure that is higher at the outer surface. This also restricts moisture transport that is achieved through convection by the gas phase. As drying proceeds towards the irreducible value, the pore water pressure decrement starts to slow down indicating that the body is in a nearly fully dry state. In general the range of computed values for the pore water pressure that is presented in Figure 6 is high. However, it is appropriate for the suction curve for concrete and cement paste that has been assigned in this case [16]. Based on the comparison with the benchmark case study as presented in this section, it can be concluded that all the results are appropriate to describe the drying process according to the selected material properties.

7.2. TWO DIMENSIONAL CASE STUDY

Based on the validation case studies described above, the simulation was extended to address the drying of a ceramic section that forms a single layer in the investment casting shell. The heat and mass transfer coefficient were chosen to be more closely similar to the shell drying process [28, 29] by specifying an ambient temperature of 22°C and a relative humidity of 50−60%. This represents nearly an isothermal drying process, but is representative of the environment for shell drying. This was done in order to demonstrate the robustness of the

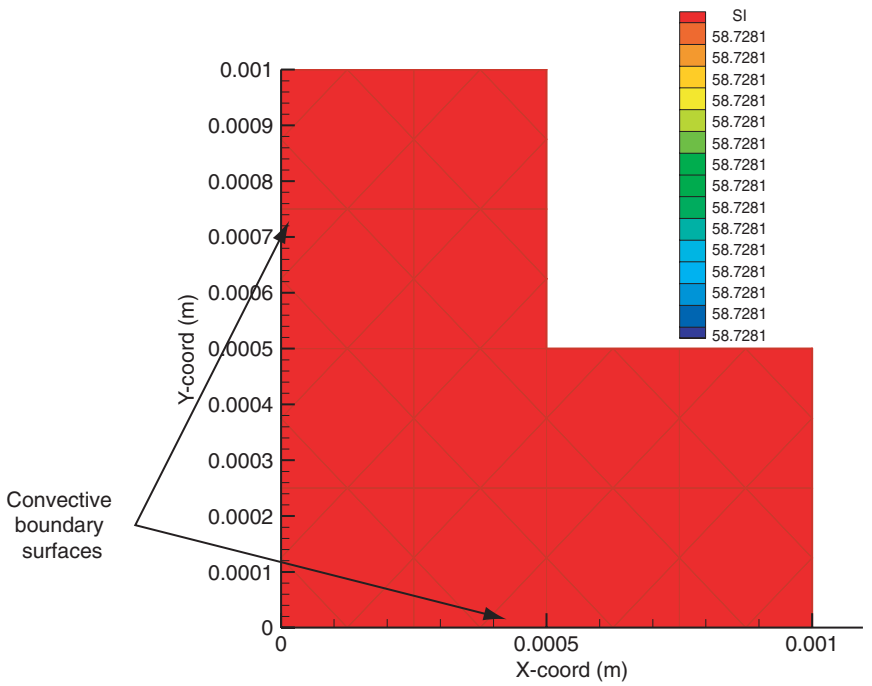

Figure 7 The domain mesh and boundary conditions for single layer with corner shape – initial condition is fully saturated.

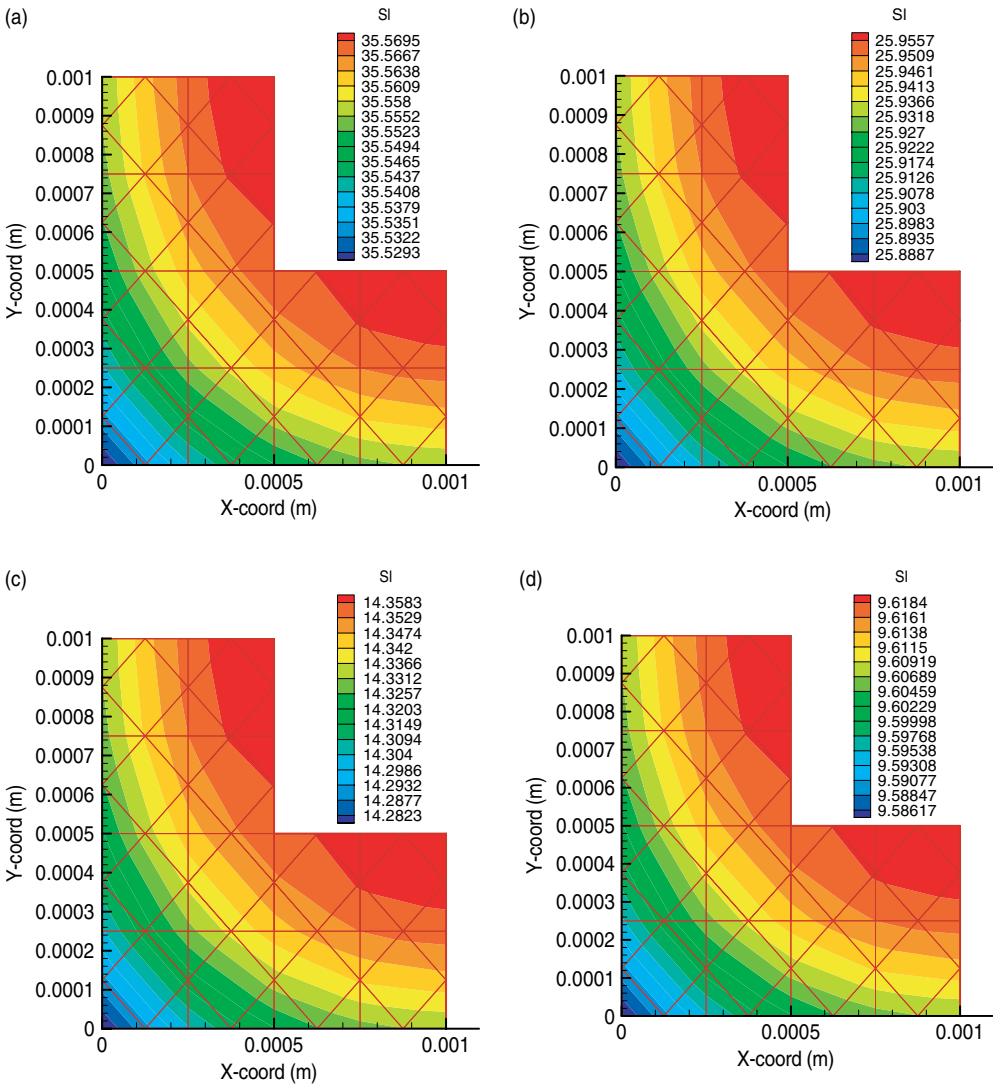

Figure 8 Saturation contours at 15 minutes (a), 30 minutes (b), 1 hour (c), 2 hours (d) of drying times for the single layer case study (corner shape).

code and also to illustrate the hygrothermal response especially in the corner zone of the thin shell layer. Sensitivity studies on mesh refinement were undertaken within this analysis [30], from which the coarse mesh as (shown in the rectangles below) was found to be sufficient. The diagonal lines are a product of the graphical presentation, they do not represent elements that were used in the analysis.

As presented in Figure 8, over the drying times as expected the greatest changes are observed in the corner zone where the saturation, permeability, relative humidity value reach their minimum value due to the convection from two adjacent sides. In the early stage of drying (constant rate period) or above the critical value (0.3), saturation drops drastically within 30 minutes. This condition indicates the capillarity effect and free water

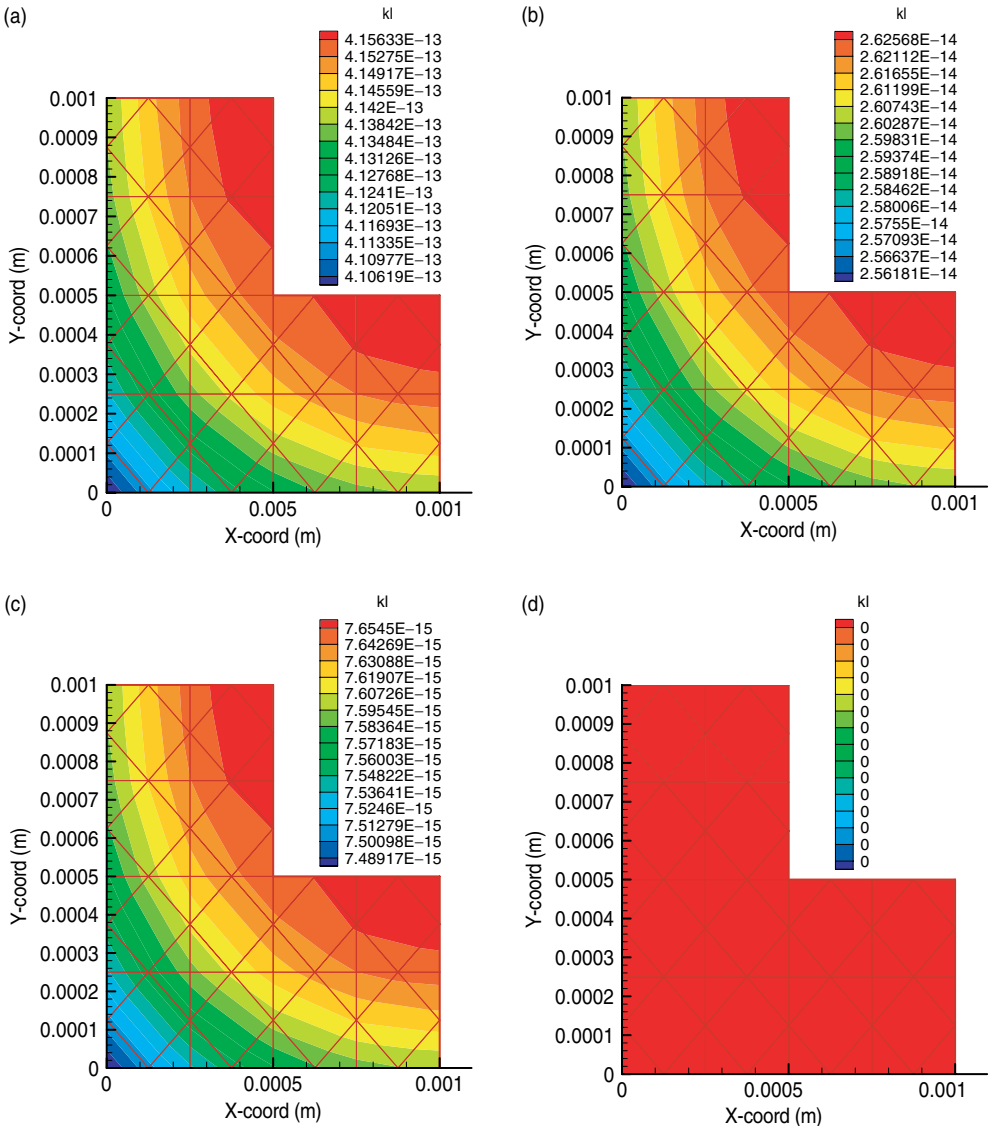

Figure 9 Permeability contours at 15 minutes (a), 30 minutes (b), 1 hour (c), 2 hours (d) of drying times for the single layer case study (corner shape).

movement that leads to the moisture loss. As drying proceeds and exceeds the critical value after 30 minutes, moisture loss slowly starts to reduce. This is clearly shown by comparing the value of saturation in Figure 8(c) and Figure 8(d) where it took nearly 1 hour to have a reduction of 8% in saturation as compared to the beginning of drying time, where its shows a 50% loss in saturation in less than 30 minutes. The corresponding trends in the liquid permeability value are presented in Figure 9. In this instance a near uniform and zero liquid permeability is achieved after sufficient drying time and the transient period shows a variation that is similar in profile to that of saturation.

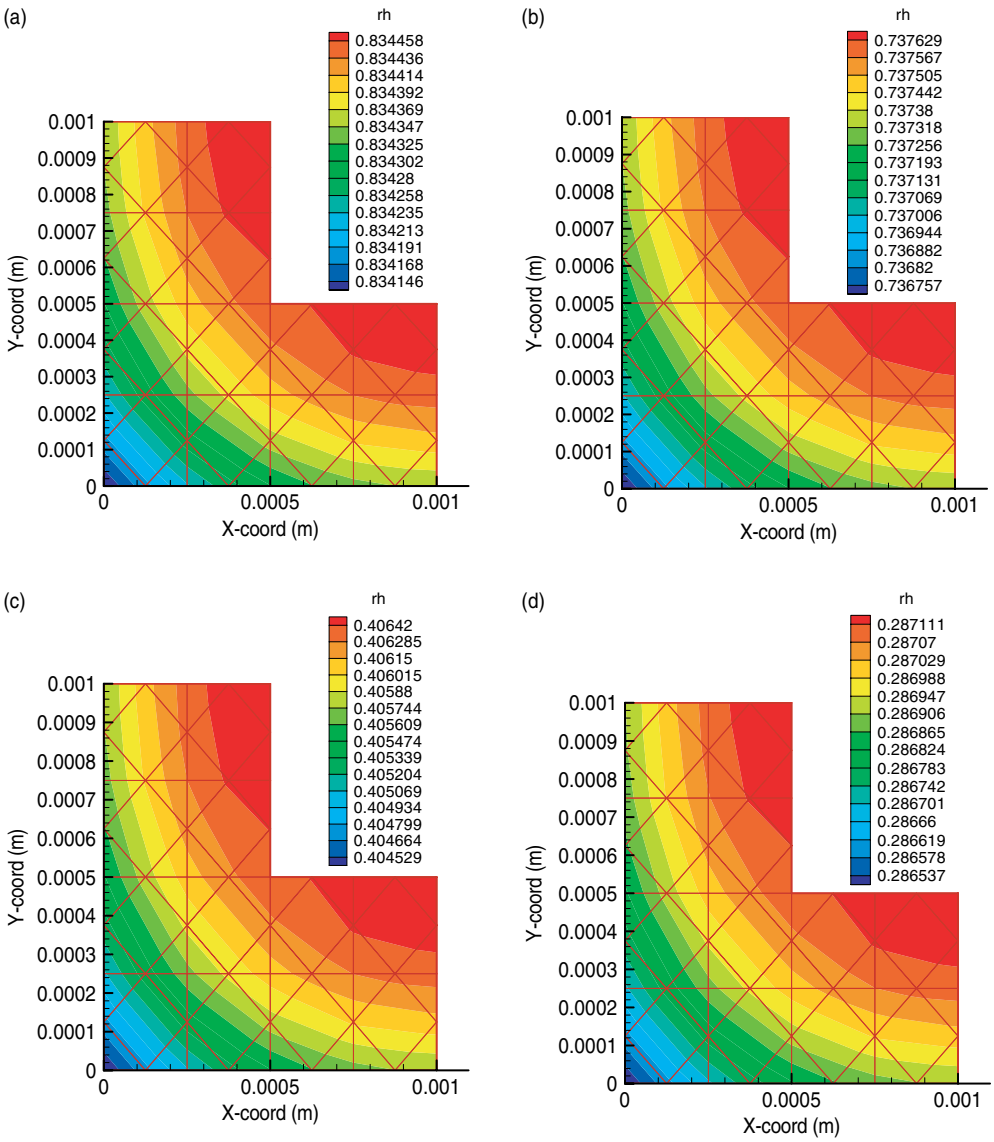

Figure 10 Relative humidity contours at 15 minutes (a), 30 minutes (b), 1 hour (c), 2 hours (d) of drying times for the single layer case study (corner shape).

Again, a similar response is presented for the relative humidity evolution as drying starts, see Figure 10. As discussed and presented for the one dimensional case study a slow change in relative humidity takes place when the moisture content is above the critical saturation. This indicates that the vapour in pore section is in near equilibrium with the ambient saturated vapour pressure and this indicates the free water movement within the porous body.

Saturation, liquid permeability and relative humidity contours show in a similar pattern due to their strong dependence on the moisture content. These can be seen clearly in Figures 8 to 10. Characteristically, all variables show a small change across the body due to the small amount

of water content in a very thin ceramic shell layer (it is 0.5 mm thick) and this is coupled with its ability to promote moisture transport. The preceding has illustrated the characteristics response for the corner section. As stated earlier, simulation can be used to explore the impact of material properties on the evolution of saturation within the body. This can be used to explore the drying rate with respect to the material property. This is important in the design of materials and in the determination of the precision with which it needs to be measured within an experimental characterization programme. An example of a sensitivity study of material property is set out below in which the impact of intrinsic permeability is explored.

7.3. MATERIAL SENSITIVITY CASE STUDY

In this instance, the plain brick study in Section 7.1 has been taken and the intrinsic permeability value is changed by an order of magnitude to $K_{intc} = 1.0 \times 10^{-17}$. The consequent impact on pore water and gas pressure is shown below in Figures 11(a) and 11(b) and these may be contrasted directly against Figures 5 and 6 respectively.

By reducing the intrinsic permeability value by a factor of 10, the results show that the evolution of pore water pressure becomes very steep along to the convective boundary with the lower permeability value. This is linked directly to the ease of liquid movement within

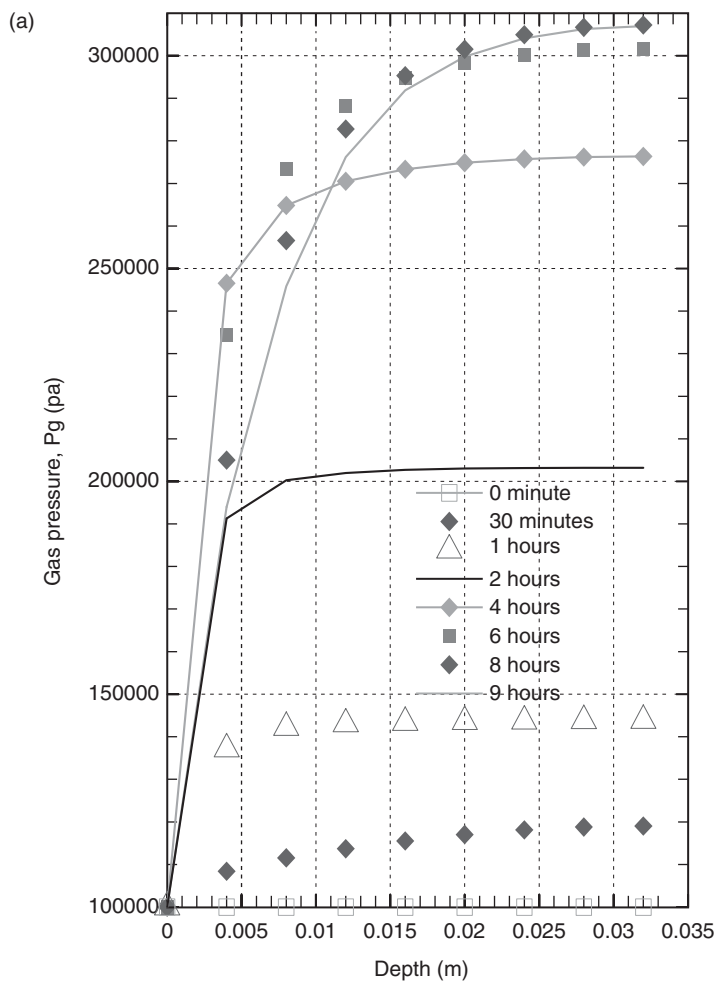

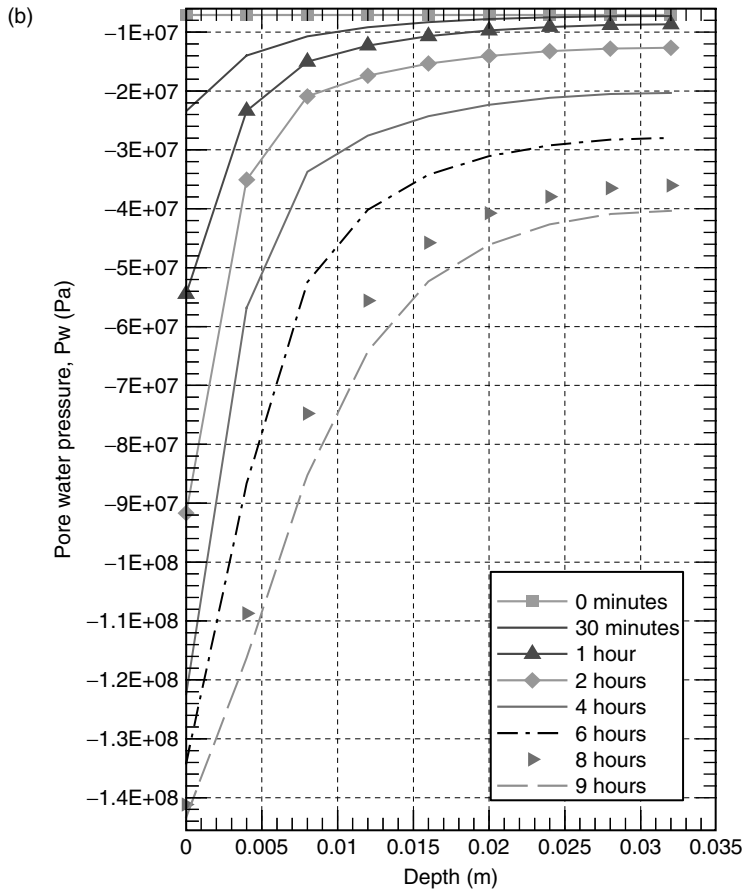

Figure 11 (a) gas pressure and (b) the pore water pressure with different time at intrinsic permeability value, $K_{intc} = 1.0 \times 10^{-17}$ (changed by a factor of 10 from the standard data).

the pore section as this is described by the permeability level and hygroscopicity of the body. Comparison of the above plots and with the standard plots in the validation case study (Figure 5 and 6), clearly show that this change will result in a higher pore water pressure and gas pressure created within the network as water is removed. Therefore the lower permeability value shows that the body has a more restricted spaces for the fluid phases, and indicates that the body is more hygroscopic. Based on this studies and comparisons that have been done, the material properties do have an impact on pore water and gas transport highlighting the need for accurate determination of these material parameters. Similar studies may be applied to other material parameters, however, in undertaking such sensitivity, it was found that numerical problems can arise with solution convergence when the material properties that and be imposed numerically lead to incompatibility that are extreme or are not physically realistic.

8. CONCLUSION

The aim of this study was to establish the basis of a simulation approach to represent the heat and mass transfer that occurs during the drying of single layer ceramic shell body. The model

used is very comprehensive and accounts for moisture transport by capillary, vapour and gas transport mechanisms and also energy transfer that includes latent heat and diffusion including the influence of local moisture content. Through benchmarking against a documented experimental study, the results show that the prediction of measured variables and transport properties are in good agreement with other related work. Verification of the model has been performed on a one dimensional domain, focusing on brick drying. This was also extended to illustrate application of material sensitivity study in which it was found that the simulation scheme was capable of undertaking this, but that there was a need to maintain the material parameters within physically realistic limits. A two dimensional study is also presented for conditions that are pertinent to shell drying conditions. This also shows a correct trend of drying stage and drying mechanism in the nonhygroscopic porous media, as similarly presented in the previous benchmark of the brick drying.

NOTATIONS

$\pm \dot{m}$	=	condensation and evaporation term, kg/m^{3}s
T	=	Temperature, °C
P	=	pressure, Pa
v	=	velocity, ms^{-1}
ρ	=	density, kg/m^3
ϕ	=	porosity
L	=	Latent heat of water vaporization (J/kg)
k_g , k_l	=	relative permeability of gas and liquid phases.
K	=	intrinsic permeability of solid phase (m^2)
C_p	=	heat capacity, J/(mol K)
χ	=	thermal conductivity(W/m K)
S	=	Saturation (%)
rh	=	relative humidity

SUBSCRIPTS

a, v, g, l, s	=	air, vapour, gas, liquid, solid
c, irr, sat	=	capillary, irreducible, saturated
∞, f	=	ambient, final

REFERENCES

[1] Whitaker, S., Simultaneous heat, mass and momentum transfer in porous media: a theory of drying, *Adv. Heat Transfer*, 1977, 13**,** 119–203.

[2] Luikov, A. V., *Heat and Mass Transfer in Capillary Porous Bodies*, Oxford Pergamon, 1975.

[3] Lewis, R. W., and Ferguson, W. J., The effect of temperature and total gas pressure on the moisture content in a capillary-porous body, *International Journal of Numerical Methods in Engineering*, 1990, 29, 357–369.

[4] Keum, Y. T., Jeong, J. H., and Auh, K. H., Finite-element simulation of ceramic drying processes, *Modelling and Simulation in Material Science Engineering*, 2000, 8, 541–556.

[5] Shusheng, P., and Keey, R. B., Modelling the temperature profiles within boards during the high-temperature drying of Pinus radiata timber: the influence of airflow reversal, *International Journal of Heat and Mass Transfer*, 1995, 38(2), 189–205.

[6] Nidjam, J. J., Langrish, T. A. G., and Keey, R. B., A high-temperature drying model for softwood timber, *Chemical Engineering Science,* 2000, 55, 3585–3598.

[7] Zhang, J., and Datta, A. K., Mathematical modelling of bread baking process, *Journal of Food Engineering*, 2006, 75(1), 78–79.

[8] Stanish, M. A, Schajer, G. S., and Kayihan, F., A mathematical model of drying for hygroscopic porous media, *AIChE*, 1986, 32(8), 1301–1311.

[9] Nasrallah, S. B, and Perre, P., Detailed study of a model of heat and mass transfer during convective drying of porous media, *International Journal of Heat and Mass Transfer*, 1988, 31(5), 957–967.

[10] Even., J, and Thomas, H. R., Heating unsaturated medium, *Geotechnique*, 1989, 39(3), 445–70.

[11] Gawin, D., Manjorana, C. E., and Schrefler, B. A., Numerical analysis of hygrothermal behaviour and damage of concrete at high temperature, *Mechanics of Cohesive Frictional Materials*, 1999, 4, 37–74.

[12] Mayhew, Y. R., and Rogers, G. F. C., *Thermodynamic and Transport Properties of Fluids*, 2nd edn., Blackwell, Oxford, 1976.

[13] Steven, A., and Grant, A. S., Calculation of temperature effects on wetting coefficients of porous solids and their capillary pressure functions, *Water Resources Research*, 1996, 32(2), 261–270.

[14] Van Genucthen, M. A., A closed-form equation for predicting the hydraulic conductivity of unsaturated soils, *Soil Science Society of America*, 1993, 44, 892–989.

[15] Morales, E. R., *Characterization and Thermo-hydro-mechanical Behaviour of Unsaturated Boom Clay: An Experimental Study*, PhD Thesis, Universitat Politecnica' De Catalunya, Barcelona, 1999.

[16] Baroghel-Bouny, V., Mainguy, M., Lassabatere, T., and Coussy, O., Characterization and identification of equilibrium and transfer moisture properties for ordinary and high performance cementitious material, *Cement and Concrete Research*, 1999, 29**,** 1225–1238.

[17] Hansen, K. K., Peuhkuri, R. H., Kristensen, A., and Hansen, E. J. D., Unfired clay bricks-retention curves and liquid diffusivities, *Building Physics 2002-6th Nordic symposium*, 2002.

[18] Keey, R. B., *Drying Principles and Practice*, Pergamon Press, Great Britain, 1975.

[19] Nissan, A. H., Kaye, W. G., and Bell, J. R., Mechanism of drying thick porous bodies during the falling rate period, *AIChE*, 1959, 5, 103–110.

[20] Skorokho, V. B., Khariton, P. M., and Dobryako, V. M., Calculation of nonlinear thermal-conductivities by Picard Method, *High Temperature*, 1973, 11(3) , 621–622.

[21] Balasubramanian, P., Suhas, H. K., and Ramamurti, V., Skyline solver for the static analysis of Cyclic Symmetrical Structures, *Computers and Structures*, 1991, 38(3), 259–268.

[22] De Vries, D. A, Simultaneous transfer of heat and moisture in porous media, *Trans Am Geophysc Union*, 1958, 39, 909–916.

[23] Spolek, G. A., and Plumb, O. A., Capillary pressure in softwood, *Wood Science and Technology*, 1981, 15**,** 189–199.

[24] Tesoro, F. O., Choong, E. T., and Kimbler O. K., Relative permeability and the porous pore structure of wood, *Wood and Fibre Science*, 1974, 6(3), 226–236.

[25] Ilic, M., and Turner, I. W., Convective drying of a consolidated slab of wet porous material, *International Journal of Heat and Mass Transfer*, 1989, 32, 2351–2362.

[26] Garwin, D., and Schrefler, B. A., Thermo-hydro-mechanical Analysis of partially saturated porous material, *Engineering Computations*, 13, 113–143.

[27] Tai Hong, V., *Influence of pore size distribution on drying behaviour of porous media by a continuous model*, PhD Thesis, Universitat Magdeburg, 2006.

[28] Leyland, S., and Jones, S., *The effect of drying conditions upon the wax/ceramic interface temperature*, Private Communication: Rolls-Royce plc.

[29] Jones, S., and Leyland, S., Investigation into the drying behaviour of water based slurries, I.C.I *42nd Annual Technical Meeting*, 1994

[30] Harun, Z., *Simulation Of Drying For Multilayer Investment Casting Shells*, PhD Thesis, University of Wales, Swansea, 2007.

ACKNOWLEDGMENT

The financial support sponsored by Tun Hussein Onn University College (KUiTTHO), Malaysia towards the research studies of first author is gratefully acknowledged.